2021 IEEE/RSJ International Conference on Intelligent Robots and Systems (IROS)
September 27 - October 1, 2021. Prague, Czech Republic

2021 IEEE/RSJ International Conference on Intelligent Robots and Systems (IROS) | 978-1-6654-1714-3/21/$31.00 ©2021 IEEE | DOI: 10.1109/IROS51168.2021.9636697

Soft Retraction Device and Internal Camera Mount for Everting Vine Robots

William E. Heap[1*], Nicholas D. Naclerio[2], Margaret M. Coad[3], Sang-Goo Jeong[4] and Elliot W. Hawkes[2]

***Abstract*— Soft, tip-extending, pneumatic "vine robots" that grow via eversion are well suited for navigating cluttered environments. Two key mechanisms that add to the robot's functionality are a tip-mounted retraction device that allows the growth process to be reversed, and a tip-mounted camera that enables vision. However, previous designs used rigid, relatively heavy electromechanical retraction devices and external camera mounts, which reduce some advantages of these robots. These designs prevent the robot from squeezing through tight gaps, make it challenging to lift the robot tip against gravity, and require the robot to drag components against the environment. To address these limitations, we present a soft, pneumatically driven retraction device and an internal camera mount that are both lightweight and smaller than the diameter of the robot. The retraction device is composed of a soft, extending pneumatic actuator and a pair of soft clamping actuators that work together in an inch-worming motion. The camera mount sits inside the robot body and is kept at the tip of the robot by two low-friction interlocking components. We present characterizations of our retraction device and demonstrations that the robot can grow and retract through turns, tight gaps, and sticky environments while transmitting live video from the tip. Our designs advance the ability of everting vine robots to navigate difficult terrain while collecting data.**

I. Introduction

Soft robots have the unique ability to change shape and passively conform to their environment to interact with unknown shapes and obstacles. One promising class of soft robots is everting vine robots, which extend from the tip, similar to how vines grow [1]. These robots can extend over 250x their initial length, move without experiencing friction with their surroundings, conform to their environment, rise up over obstacles, and pass through narrow apertures [2]. With these advantages, vine robots can be used in situations where delicate interaction is required [3], where humans and robots cooperate [4], and where it is difficult for humans and other robots to explore [5].

Vine robots are made of a thin-walled tube of flexible material that is folded inside itself. When pressurized, the internal material, or "tail," is drawn to the tip of the robot where it everts, or turns inside out, and becomes part of the outer wall. To retract, the tail is pulled toward the robot base to invert the outer wall and shorten the robot.

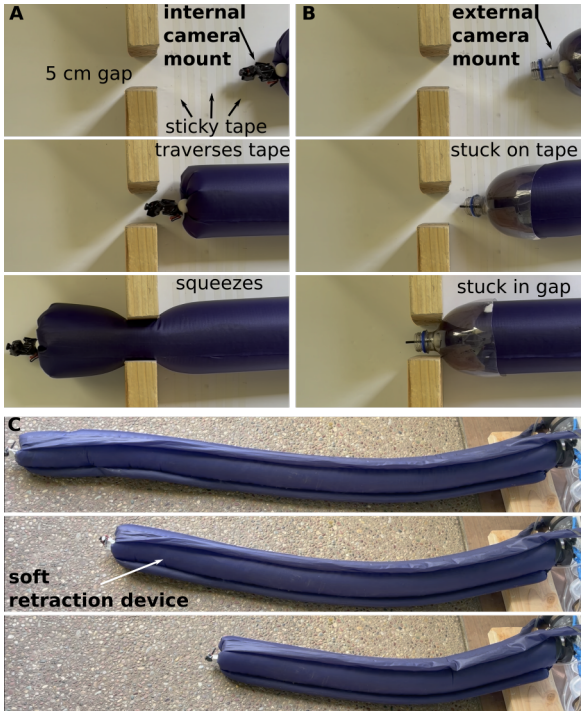

Fig. 1. Our internal camera mount and soft retraction device. (A) With our internal camera mount, a 10 cm diameter vine robot can pass over sticky tape and squeeze through a 5 cm wide gap. (B) An external camera mount gets stuck on the same tape and gap. (C) Our soft retraction device enables successful retraction. See the accompanying video.

In many vine robot applications, it is important to reverse the robot's growth without bending or buckling the robot body, and to mount sensors or tools at the robot tip to sense or interact physically with the environment. For example, the robot may need to explore multiple branching paths while transmitting video to a human operator, or the robot may need to retract to avoid obstacles while carrying a gripper at its tip to manipulate objects. However, existing solutions diminish some of the advantages of vine robots and thus fall short for some applications.

Prior work has addressed the challenge that vine robots, particularly long or curved ones, tend to bend or buckle undesirably when retracted from the base [6], [7]. One method is to add a stiffening element inside the robot body [7], but this is effective only at short lengths since the force required

This work was supported by the NSF (grant #1944816) and UC Santa Barbara Undergraduate Research and Creative Activities (grant #3882). The work of N.N. was supported by a NASA Space Technology Research Fellowship, and the work of M.C was supported by an ARCS Foundation fellowship.

[1]College of Engineering, University of California, Santa Barbara, CA 93106 USA
[2]Department of Mechanical Engineering, University of California, Santa Barbara, CA 93106 USA
[3]Department of Aerospace and Mechanical Engineering, University of Notre Dame, Notre Dame, IN 46556 USA
[4]Department of Civil and Environmental Engineering, Korea Advanced Institute of Science and Technology (KAIST), Daejeon-si, Republic of Korea
*Corresponding author. Email: wheap@ucsb.edu

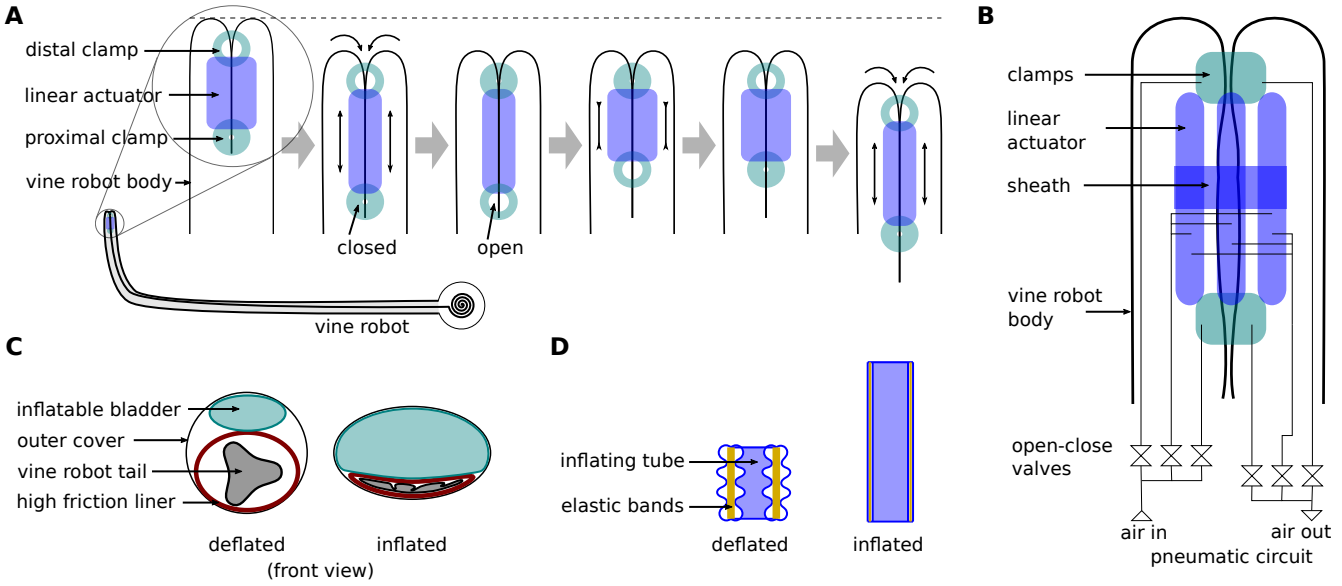

Fig. 2. Retraction mechanism design and operation. (A) Retraction operation sequence. While the proximal clamp is closed and the distal one open, the linear actuator extends, inverting the robot. The distal clamp closes while the proximal one opens and the linear actuator contracts, enabling a new cycle. (B) Retraction mechanism layout and pneumatic circuit. Note that the linear actuator is made up of four tubes, with the one directly behind the center one not shown. (C) Soft clamp design. (D) Extensile pneumatic linear actuator design.

to buckle decreases with length. A method that works at any length is to use a "retraction device" to retract from the robot tip instead of the base. However, previous electromechanical designs that pull the tail through two motor-driven rollers [6], [8] are limited in power density, force, speed, and weight.

Attaching sensors and tools to the tip of a vine robot is challenging because the material at its tip changes as the robot grows and retracts. Various designs have addressed this issue [2], [4], [5], [8], [9], [10]. However, as discussed in detail in [8], each design has its own benefits and drawbacks, and no design has been developed that can satisfy all the following conditions: (1) remains at the robot tip during growth and retraction, (2) transmits pulling forces to the environment, (3) functions at arbitrary robot lengths, (4) incorporates retraction without bending/buckling, (5) adds minimal weight to the robot tip, (6) avoids sliding relative to the environment, and (7) allows body shrinking through apertures.

To address these gaps, we developed a novel retraction device and internal camera mount design (Fig. 1). Our retraction device maintains the benefits of previous designs, but in a soft, pneumatic form. Our camera mount fits inside the robot, rather than surrounding the tip, which means the robot does not slide against the environment during growth or retraction, can pass over sticky obstacles, and can squeeze through apertures smaller than its body diameter while carrying a camera at its tip. Further, with comparable output power and 40% the weight of [8], our design can better lift over obstacles. In this paper, we present the design, modeling, fabrication, and experimental characterization of both the retraction device and camera mount.

II. Design and Modeling

Our retraction device is shown in Fig. 2, and our internal camera mount is shown in Fig. 4. These two systems can be used together as demonstrated here, or independently. The soft retraction device is composed of a pair of clamps and a linear actuator, while the camera mount is composed of an internal and external frame. This section explains the method of retraction, and the design and modeling considerations of each component.

A. Retraction Device

1) Method of Retraction: The soft retraction mechanism fits inside the tip of the robot, and pulls on the tail material to invert and retract the robot without bending or buckling. The mechanism is composed of two pneumatic clamps connected by an extensile pneumatic linear actuator (Fig. 2). The retraction mechanism is driven in an inchworm motion similar to a shuffling rope pull, shown in Figs. 2A and 3. To initiate a retraction cycle, the proximal clamp is closed while the distal clamp is opened. Next, the linear actuator extends, driving the proximal clamp away from the tip of the robot, causing the robot to invert. Then, the distal clamp is closed, and the proximal clamp is opened. Lastly, the linear actuator contracts, pulling the proximal clamp towards the tip of the robot. The cycle can now repeat, with additional vine robot material inverting each cycle.

2) Soft Clamp Working Principle: The two soft pneumatic clamps at each end of the retraction mechanism grasp the tail of the vine robot (Fig. 2B). Each clamp is composed of an inextensible inflatable bladder and a high friction liner surrounded by an inextensible outer cover (Fig. 2C). The tail of the robot passes through the high friction liner. When the clamp is open, the robot tail can pass freely through the

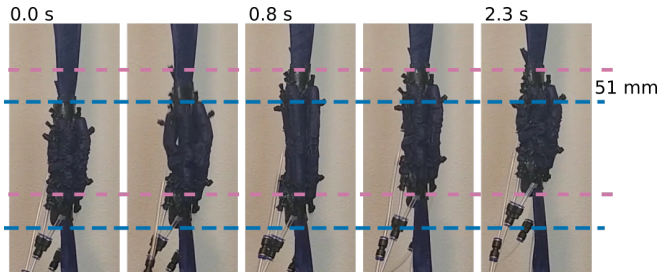

Fig. 3. The actuation pattern of the linear actuator, as in Fig. 2A. The actuator moves along a section of vine robot material in a series of extensions and contractions. See the accompanying video.

clamp. As the clamp's bladder inflates, it squeezes the high friction liner against the robot tail, holding it in position.

Once the clamp is inflated enough to fully contact the tail of the vine robot, friction between it and the robot tail is expected to increase linearly with pressure, given a constant coefficient of friction. This friction force F_{clamp} is

$$F_{clamp} = \mu PA, \tag{1}$$

where μ is the coefficient of friction between the clamp and the vine robot tail, P is the clamp pressure, and A is the contact area between the clamp and tail (assumed to be constant after maximum contact is made at low pressure). This means that the friction force between the clamp and the tail can be tuned by varying the pressure. At high pressure, the clamp prevents movement of the tail through the clamp, at zero pressure it allows movement, and at an intermediate pressure the clamp acts like a braking clutch.

3) Linear Actuator Working Principle: Between the two clamps is a soft extensile pneumatic linear actuator that drives the movement of the retraction device. Prior soft, extensile, pneumatic actuators include elastic [11], origami [12], and braided [13] designs. Our linear actuator is composed of four airtight tubes arranged radially around the tail of the vine robot, which lengthen as they are pressurized (Fig. 2B). A sheath surrounds the four tubes to limit buckling. Each tube has three elastic bands spanning its length, arranged radially around its circumference (Fig. 2D). These bands provide a restorative force to shorten the tube when depressurized. The force provided by the actuator is the force of the inflating tubes minus the restorative force of the elastic bands. The force required to retract the robot from the tip was found in [6] to be the vine body pressure times its cross-sectional area plus a term for material stiffness.

Because the linear actuator buckles during normal operation but is restrained by a sheath, the force exerted by the linear actuator is less than that of a pneumatic cylinder, but more than that of an axially buckled inflated beam of the same size. An inflated beam will buckle in axial loading when the applied load exceeds a critical value F_{cr} [14] which is

$$F_{cr} = \frac{EI\frac{\pi^2}{L^2}(P\pi r^2 + G\pi rt)}{EI\frac{\pi^2}{L^2} + P\pi r^2 + G\pi rt} \tag{2}$$

where P is internal pressure, E is elastic modulus, G is shear modulus, I is area moment of inertia of a cylindrical shell ($\pi r^3 t$), L is length, r is radius, and t is material thickness. If the shear stiffness of the material is very weak, as in a single layer of woven fabric,

$$F_{cr} \to P\pi r^2 + G\pi rt. \tag{3}$$

However, in our case when the beam is not fully extended, its walls are wrinkled, slack, and cannot hold tension. Therefore $E \to 0$ and

$$F_{cr} \to 0. \tag{4}$$

Thus, our inflating beams will always buckle (when not fully extended).

The restorative moment, τ applied by a buckled inflated beam is πPr^3 [15]. The axial force component of this buckling moment F_b is

$$F_b = \frac{\pi Pr^3 \sin\theta}{L/2}. \tag{5}$$

where θ is the angle that the beam is bent from linear. The force exerted by a pneumatic cylinder is simply PA, where A is cross-sectional area. Thus, the total force exerted by the linear actuator $F_{actuator}$ can be written as

$$F_b - F_e(x) < F_{actuator} < PA - F_e(x), \tag{6}$$

where $F_e(x)$ is the restorative force of the elastic bands, which depends on their displacement x from their natural length. Equation (6) does not take into account effects by the elastic bands in helping to prevent buckling, but this effect should be minor.

The maximum pressure that the linear actuator can withstand before bursting is limited by material strength, which is quantified using the material's yield stress σ_y. Using hoop stress at yield to determine burst pressure ($P_{max} = \sigma_y t/r$), the maximum force (PA) that an actuator can exert is

$$F_{max} = \pi\sigma_y rt. \tag{7}$$

Four inflated beams have the same cross-sectional area as a single inflated beam with double the radius. Thus, for a given cross-sectional area, material, and thickness, the F_{max} with four cylinders is twice that of a single one.

4) Linear Actuator Power Scaling: The power of a pneumatic actuator is limited only by its air supply. Pneumatic power is $P\ dV/dt$, where P is pressure and dV/dt is volumetric flow rate, a property of the air supply. Given that $P_{max} = \sigma_y\ t/r$, and dV/dt is proportional to r^2, for a given σ_y, power is proportional to tr. Power therefore scales linearly with mass to the two-thirds power, while the power of an electric motor scales linearly with mass [16].

B. Camera Mount

The camera mount is composed of two components: the external frame which sits inside the tail of the vine robot and extends outside the tip to hold the camera, and the internal frame which rides along inside the pressurized part of the robot body. The external frame is a rod with two spheres:

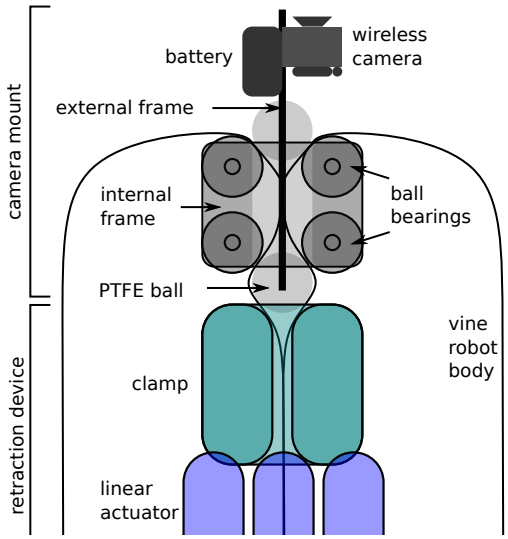

Fig. 4. Details of the camera mount design. The external frame of the camera mount is inside the tail of the vine robot, while the internal frame is inside the pressurized part of the robot body. These parts are interlocked, keeping them in place at the tip of the robot. The vine robot body passes between the ball bearings and PTFE balls, which are both designed to have low friction.

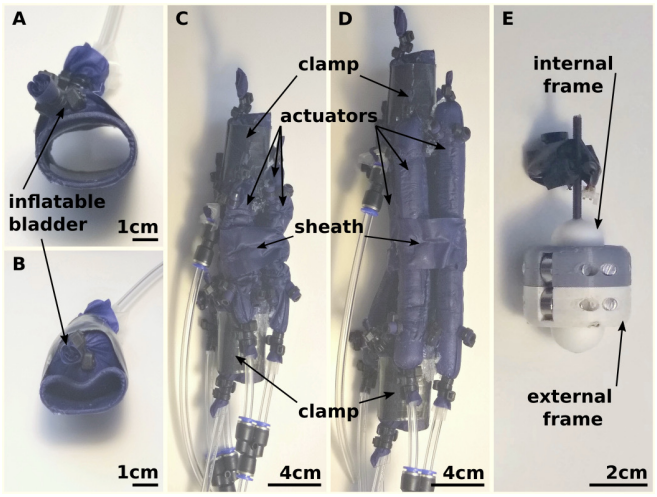

Fig. 5. Photos of the retraction device and camera mount components, as shown in Figs. 2 and 4. The (A) deflated and (B) inflated retraction device clamps. The (C) deflated and (D) inflated retraction device linear actuator. (E) The camera mount with a wireless camera at its tip.

one at its proximal end, and the other at the center, with the camera at the distal end, as shown in Figs. 4 and 5E. The internal frame is a cylinder with a ring of bearings at both ends. The internal frame and external frame interlock, allowing the tail material to pass in between in a low friction manner.

This design was chosen to minimize the diameter of the camera mount and keep all but the camera inside the body of the robot. Further, because the inner and outer frames are physically interlocked, the camera mount will not fall off and can apply tension on the environment. Due to its small diameter, the camera mount's orientation can vary relative to the orientation of the robot body wall, but if there is tension on the tail, it stays relatively straight.

III. Fabrication

A. Retraction Device

The retraction device consists of two separate components: the clamps and the linear actuator (Fig. 5). Both components utilize identical inflatable, bi-layer, tube-shaped bladders for pneumatic actuation. The airtight inner layer is a 50 µm thick thermoplastic polyurethane (TPU) film (American Polyfilm). The outer layer is a silicone and urethane impregnated, nominally 50 µm thick, 30 Denier ripstop nylon fabric (Seattle Fabrics) bonded with room-temperature vulcanizing silicone adhesive (SilPoxy, Reynolds Advanced Materials). This fabric will be referred to as "silnylon." Each bladder is supplied air by a 6.4 mm (1/4") outer diameter, 3.2 mm (1/8") inner diameter PVC plastic tube.

The two clamps used in the retraction device are identical, and are each composed of an inflatable bladder, an inextensible outer cover, and a high friction liner as shown in Fig. 2C. The bladder, as described above, is 140 mm in diameter. The outer cover is a 0.2 mm thick, 31.8 mm outer diameter 70 Denier thermoplastic polyurethane coated rip-stop nylon (Seattle Fabrics). The high friction liner is a 3.2 mm thick, 25 mm outer diameter silicone tube (5236K237, McMaster-Carr). Both the bladder and the inextensible outer cover are 38 mm long, while the high friction liner is 51 mm long, leaving room to attach the actuator to the clamps. To reduce friction when the vine robot tail enters and exits an open clamp, a sheet of silnylon is adhered to the outer edges of the high friction liners and extends 6 mm into the inside of the high friction liner.

The linear actuator is comprised of four inflating tubes attached to the clamps at their ends, and with a sheath of silnylon around their center. Each inflating tube is a bladder as described above, 19 mm in diameter and 127 mm in length. To compress them, each tube has three 63.5 mm long latex tubes (260Q, Qualatex) running symmetrically along its length, attached with a layer of silnylon. A 50.8 mm long, 57 mm diameter silnylon sheath is adhered around the center of the four bladders as shown in Figs. 2B and 5. The retraction device, excluding the pneumatic tubing that connects to the vine robot base, has a mass of 132 g.

B. Camera Mount

The camera mount is composed of an internal, and an external frame. The internal frame is made of two identical 3D-printed housings screwed together. Each housing has three 12.7 mm (1/2") outer diameter ball bearings mounted on 9.5 mm (3/8") aluminum axles. The distal face of the internal frame is coated with PTFE tape (6305A42, McMaster-Carr) to reduce friction with the robot body. The external frame is composed of two 25.4 mm (1") diameter PTFE balls (9660K33, McMaster-Carr) press-fit onto a 3.2 mm (1/8") diameter carbon fiber rod. The PTFE balls press against the bearings of the internal frame without fitting through.

The distal PTFE ball can be removed to remove the camera mount from the vine robot body, while the proximal PTFE ball can withstand up to 5.5 N of tension before slipping off the carbon fiber rod. A camera and wireless transmitter (WT05 Micro, Wolfwhoop) and a 3.7 V, 220 mAh battery (35C, Makerfire) were attached to the carbon fiber rod with electrical tape and used to record video. The mass of the camera mount without a camera or battery is 54 g.

C. Vine Robot Body

The vine robot bodies used in our experiments were made of silnylon for its conformability and low friction. The robot was steered by three fabric pneumatic artificial muscles, as described in [17] and shown in [18], arranged radially around its body. The robot's base was as described in [5].

IV. Experimental Results

A. Clamp Characterization

The holding force produced by the retraction device's clamp increases roughly linearly with bladder pressure. We measured the force required to pull the vine robot tail material through a clamp, as a function of its inflatable bladder pressure. Three trials were conducted at each pressure. As shown in Fig. 6A, the force increased in a superlinear manner until about 80 kPa, after which it increased linearly, as expected by (1). The superlinear trend is likely caused by increasing contact area as the bladder inflates.

B. Linear Actuator Characterization

The force exerted by the retraction device's linear actuator decreases with strain, and increases with pressure. The actuator was fixed to a test bed as tensile and compressive forces were measured with a digital force gauge (HF-50, Beslands) at various inflation pressures and elongations. Three trials were conducted at each position and pressure. The results are shown in Fig. 6B. At zero pressure, a negative (tensile) force was exerted by the elastic bands in the linear actuator. As pressure was increased, force increased roughly linearly, maintaining a similar slope as a function of elongation. This supports (6), which posits that the net force of the actuator is the inflation force minus the linear elastic force.

C. Effect of Shroud Length on Actuator Performance

To explore how buckling affects actuator performance, we measured its force as a function of elongation with different sheath lengths. We performed the same experiment as in Section IV-B, at a constant pressure of 24 kPa with three different shroud lengths: a full shroud the length of the actuator, a partial shroud around its middle as described in Section III-A, and no shroud. As shown in Fig. 6C, when the actuator was fully shrouded to reduce buckling, its behavior was closest to PA. With a partial shroud, its force decreased slightly, but maintained the same slope. With no shroud, force decreased by half or more, especially at low elongations, because the actuator buckles outward without a shroud, bringing its force profile closer to (5). The restorative moment of the elastic bands may also prevent the actuator from buckling.

While it increases extensile force, a full shroud prevents the linear actuator from compressing back to the same length as with the partial shroud due to the force needed to compress the extra fabric. The full shroud increases the actuator's minimum length from 64 mm to 75 mm. Fig. 6D compares the work cycles of the actuator with a full vs. partial shroud.

D. Pressure to Grow

The pressure required to grow the vine robot increased with the addition of the retraction device and camera mount. We measured the average pressure required to begin growth in a 113 mm diameter robot body (without steering muscles) over three trials. The average pressure required to grow without the camera mount or retraction device was $<$0.07 kPa (the minimum detectable by our pressure sensor). With the camera mount it was 0.46 ± 0.04 kPa, with the retraction device it was 0.57 ± 0.04 kPa, and with both the camera mount and retraction device it was 0.74 ± 0.04 kPa. Adding the camera mount in front of the retraction device reduces the friction of the vine body material entering the retraction device, thus the pressure to grow with both components is less than the sum of pressures required to grow separately.

E. Retraction Speed and Output Power

For a given retraction device pressure, retraction device speed decreases with vine body pressure, while output power increases. We measured retraction speed in a 98 mm diameter robot body (without steering muscles) at various robot body pressures (as measured at the tip of the robot). Tests were repeated with and without the camera mount for three trials. The pressure for the retraction device's clamps and linear actuator were approximately 103 kPa and 69 kPa respectively. Output power was computed as PA times the average retraction speed. The results in Fig. 7 show that retraction speed decreases with body pressure, as expected by the increased force needed to retract. Retraction speed increases slightly with the addition of the camera mount because its shape helps to route the body into the retraction device, and reduces friction, as seen by the pressure to grow results.

We also calculated the output power of the device as $PA*v$, vine body pressure times area times retraction speed, shown in Fig. 7. The power increases with body pressure, approaching 0.12 W, the same output power as the electromechanical device in [6] (based on $P=1.5$ kPa, $D=81$ mm, $v=1.7$ cm/s).

The linear actuator provides maximum output power when $PA*v$ is maximized. As P drops, v does not increase quickly enough to offset the decrease in force applied, and thus the power output drops.

F. Single Actuation Power

The average power output of a single expansion of the linear actuator was measured under three loading conditions. The time required for the actuator to pull a load a certain distance was recorded and used to calculate average

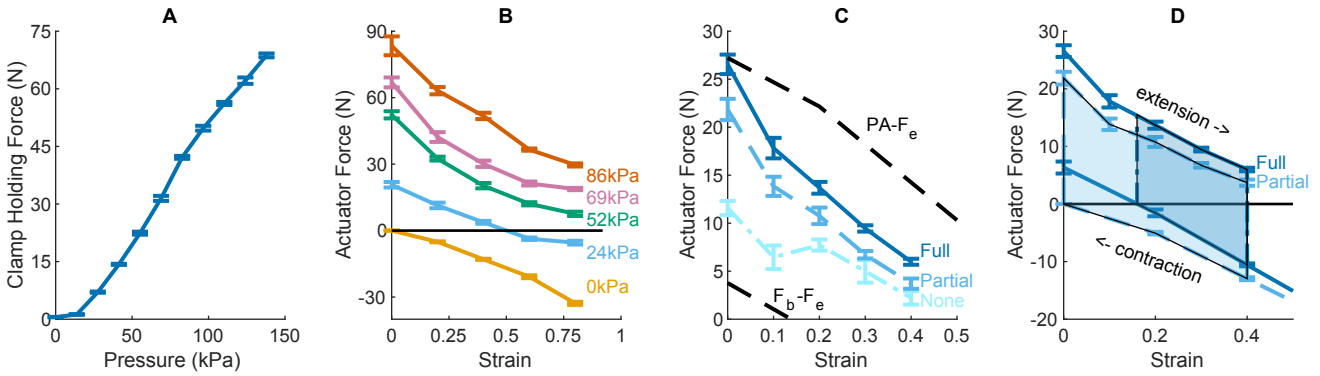

Fig. 6. Characterization of clamp and linear actuator force capabilities. (A) Holding force exerted by the retraction device's clamp as a function of bladder pressure, showing a roughly linear relationship. (B) Force exerted by the retraction device's linear actuator as a function of elongation and inflation pressure. Negative force values are in tension, while positive force values are in compression. (C) Force exerted by the linear actuator at 24 kPa as a function of elongation with a full length sheath, a partial sheath, and no sheath to prevent buckling. The device force is between that of a linear actuator, PA minus the elasticity of the elastic bands, F_e (upper dotted line), and a beam buckling actuator with the elastic bands $F_b - F_e$ (lower dotted line). F_e is the force from (B) at 0 kPa. (D) Actuator extension force at 24 kPa, and contraction force at 0 kPa with a full, and partial sheath. Shaded regions denote the two different inflation-deflation work cycles. Actuator force is increased with a full sheath at the expense of strain and work per inflation.

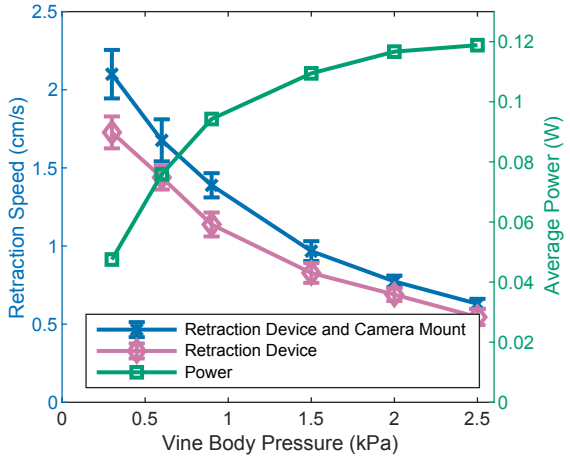

Fig. 7. Retraction speed with and without the camera mount, and output power (with camera mount) as a function of vine body pressure.

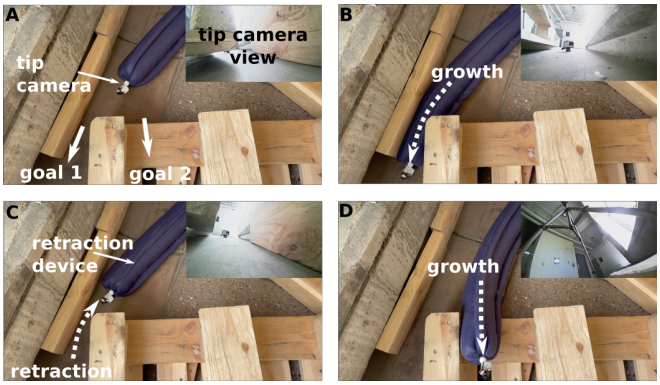

Fig. 8. Demonstration of the soft retraction device with internal camera mount growing and retracting through a narrow gap, then up and over an obstacle. The tip camera feed is inset in the top right. See the accompanying video.

power during extension. The actuator had a pressure of approximately 70 kPa, and its average power output was 0.59±0.08 W with a 5 N load, 0.54±0.01 W with a 10 N load, and 0.52±0.03 W with a 15 N load. The 0.12 W output power from Section IV-E is approximately 23% of a single 0.52 W actuation. The expansion stage takes up 0.6 s, or 25% of the 2.4 s retraction cycle.

Since pneumatic power is $P\ dV/dt$, we could increase output power by increasing either pressure or flow rate. The yield pressure of the linear actuator is 207 kPa, three times higher than the pressure used in Section IV-E, so the device could theoretically output 0.36 W by operating just under its yield pressure. Power could also be increased with larger supply tubes for higher flow rates, stronger construction for higher pressure, and optimized cycle timing for increased efficiency.

G. Demonstrations

With the internal camera mount and soft retraction device, the robot can better traverse difficult obstacles than with previous camera mount and retraction device designs. Because its components are internal, the robot was able to grow over sticky tape, while an external camera mount got stuck (Fig. 1A and B and accompanying video). Further, because the camera mount and retraction device are narrower than the robot's outer diameter, the 10 cm diameter robot was able to squeeze through a 5 cm gap, while the external camera mount could not. The mass of our combined retraction device and camera mount is under 200 g, while the tip mount in [8] is 500 g. This makes it easier to rise over obstacles. Using the retraction device and camera mount, the vine robot navigated through an obstacle course. As shown in Fig. 8 and the accompanying video, the vine robot first squeezed through a narrow gap, then retracted, then used its pneumatic muscles to turn and steer up and over another obstacle. Live video was streamed wirelessly from the camera at its tip.

V. Conclusion and Future Work

In this paper, we presented a soft retraction device and internal camera mount for everting vine robots that improves upon previous designs and advances the ability of vine robots to navigate difficult terrain while collecting data. At the pressures we tested, our retraction device produced comparable power to previous electromechanical retraction devices. Power and retraction speed could be improved by operating at a higher pressure and optimizing its extension-contraction cycle. The softness of the retraction device is also a benefit, as it makes the vine robot more robust during contact with uncertain environments. Our internal camera mount improves upon previous designs because it allows the robot to squeeze through gaps smaller than its body diameter and navigate terrain without friction against the environment, a key benefit of vine robots. The relatively light weight of our combined retraction device-camera mount design allows lifting the robot tip against gravity.

In future work, we will explore making the internal camera mount soft, allowing the robot to be entirely soft. Also, we will use image processing or explore methods to lock the orientation of the camera relative to the robot body. In addition, although they are not soft, air motors could be explored further for tethered robots [19]. They could be useful in certain situations like vine robots where a heavy compressor at the base is an acceptable trade off for a higher power density actuator at its tip.

References

[1] L. H. Blumenschein, M. M. Coad, D. A. Haggerty, A. M. Okamura, and E. W. Hawkes, "Design, modeling, control, and application of everting vine robots," *Frontiers in Robotics and AI*, vol. 7, p. 153, 2020. [Online]. Available: https://www.frontiersin.org/article/10.3389/frobt.2020.548266

[2] E. W. Hawkes, L. H. Blumenschein, J. D. Greer, and A. M. Okamura, "A soft robot that navigates its environment through growth," *Science Robotics*, vol. 2, no. 8, p. eaan3028, 2017.

[3] J. Choi, S. Lee, J. Kim, M. Lee, K. Kim, and H. In, "Development of a pneumatically-driven growing sling to assist patient transfer," in *2020 IEEE/RSJ International Conference on Intelligent Robots and Systems (IROS)*, 2020, pp. 8773–8780.

[4] F. Stroppa, M. Luo, K. Yoshida, M. M. Coad, L. H. Blumenschein, and A. M. Okamura, "Human interface for teleoperated object manipulation with a soft growing robot," in *2020 IEEE International Conference on Robotics and Automation (ICRA)*, 2020, pp. 726–732.

[5] M. M. Coad, L. H. Blumenschein, S. Cutler, J. A. Reyna Zepeda, N. D. Naclerio, H. El-Hussieny, U. Mehmood, J. H. Ryu, E. W. Hawkes, and A. M. Okamura, "Vine robots: Design, teleoperation, and deployment for navigation and exploration," *IEEE Robotics Automation Magazine*, vol. 27, no. 3, pp. 120–132, 2020.

[6] M. M. Coad, R. P. Thomasson, L. H. Blumenschein, N. S. Usevitch, E. W. Hawkes, and A. M. Okamura, "Retraction of soft growing robots without buckling," *IEEE Robotics and Automation Letters*, vol. 5, pp. 2115–2122, 2020.

[7] T. Takahashi, M. Watanabe, K. Tadakuma, M. Konyo, and S. Tadokoro, "Retraction mechanism of soft torus robot with a hydrostatic skeleton," *IEEE Robotics and Automation Letters*, vol. 5, no. 4, pp. 6900–6907, 2020.

[8] S.-G. Jeong, J.-H. Ryu, M. M. Coad, L. H. Blumenschein, M. Luo, U. Mehmood, J.-H. Kim, and A. M. Okamura, "A tip mount for transporting sensors and tools using soft growing robots," in *2020 IEEE/RSJ International Conference on Intelligent Robots and Systems (IROS)*, Oct 2020, pp. 8781–8788.

[9] D. Mishima, T. Aoki, and S. Hirose, "Development of pneumatically controlled expandable arm for search in the environment with tight access," in *Field and Service Robotics*. Springer, 2006, pp. 509–518.

[10] J. Luong, P. Glick, A. Ong, M. S. deVries, S. Sandin, E. W. Hawkes, and M. T. Tolley, "Eversion and retraction of a soft robot towards the exploration of coral reefs," in *IEEE International Conference on Soft Robotics*, 2019, pp. 801–807.

[11] A. D. Marchese and D. Rus, "Design, kinematics, and control of a soft spatial fluidic elastomer manipulator," *The International Journal of Robotics Research*, vol. 35, no. 7, pp. 840–869, 2016.

[12] R. V. Martinez, C. R. Fish, X. Chen, and G. M. Whitesides, "Elastomeric origami: programmable paper-elastomer composites as pneumatic actuators," *Advanced functional materials*, vol. 22, no. 7, pp. 1376–1384, 2012.

[13] J. Garbulinski, S. C. Balasankula, and N. M. Wereley, "Characterization and analysis of extensile fluidic artificial muscles," in *Actuators*, vol. 10, no. 2. Multidisciplinary Digital Publishing Institute, 2021, p. 26.

[14] W. Fichter, *A theory for inflated thin-wall cylindrical beams*. National Aeronautics and Space Administration, 1966, vol. 3466.

[15] R. Comer and S. Levy, "Deflections of an inflated circular-cylindrical cantilever beam," *AIAA journal*, vol. 1, no. 7, pp. 1652–1655, 1963.

[16] J. Winslow, V. Hrishikeshavan, and I. Chopra, "Design methodology for small-scale unmanned quadrotors," *Journal of Aircraft*, vol. 55, no. 3, pp. 1062–1070, 2018.

[17] N. D. Naclerio and E. W. Hawkes, "Simple, low-hysteresis, foldable, fabric pneumatic artificial muscle," *IEEE Robotics and Automation Letters*, vol. 5, no. 2, pp. 3406–3413, 2020.

[18] M. Selvaggio, L. Ramirez, N. Naclerio, B. Siciliano, and E. Hawkes, "An obstacle-interaction planning method for navigation of actuated vine robots," in *2020 IEEE International Conference on Robotics and Automation (ICRA)*. IEEE, 2020, pp. 3227–3233.

[19] S. R. Pandian, F. Takemura, Y. Hayakawa, and S. Kawamura, "Control performance of an air motor-can air motors replace electric motors?" in *Proceedings 1999 IEEE International Conference on Robotics and Automation (Cat. No. 99CH36288C)*, vol. 1. IEEE, 1999, pp. 518–524.